Chapter 2

Synthesis and Characterization of (1-x)BiFeO$_3$-xSr(Fe$_{0.5}$Nb$_{0.5}$)O$_3$ Samples

2.1 Introduction

In this chapter, we present the details of synthesis of phase pure $(1-x)BiFeO_3$-$xSr(Fe_{0.5}Nb_{0.5})O_3$ [$(1-x)BF-xSFN$] solid solutions in the composition range $0.1 \leq x \leq 1.0$ by solid state synthesis method. The synthesis of phase pure $BiFeO_3$ has been all along a challenge because of formation of unwanted impurity phases such as $Bi_2Fe_4O_9$ [Kumar et al. (2000)], $Bi_{25}FeO_{39}$ [Lebeugle et al. (2007)] and $Bi_{36}Fe_2O_{57}$ [Pradhan (2005)] during calcinations and sintering stages. The $Bi_2Fe_4O_9$ (Bi-deficient) and $Bi_{25}FeO_{39}$, $Bi_{36}Fe_2O_{57}$ (Bi-excess) impurities appear during the calcination process of compositions at $BiFeO_3$ end in BF-xSFN solid solution. To avoid the formation of these impurities, we have optimized the calcination temperature and time. There were no impurity phases at the calcination stage for the SFN end compositions. The intermediate compositions of $(1-x)BF-xSFN$ were also calcined successfully without impurities at optimized temperature. The sintering of pellets was carried out in the sealed alumina crucibles to avoid the loss of bismuth oxide. The powder of same composition was used as a spacer powder to control the evaporation of Bi during the sintering of $0.10 \leq x \leq 1.00$ compositions. We discuss in following sections the synthesis process and results of optimization of calcination and sintering stages of $(1-x)BF-xSFN$ ceramic compositions.

2.2 X-ray Diffraction for Phase analysis

X-ray diffractometer is a powerful instrument used to characterize and identify the different phases present in any material. There are various benefits of X-ray powder diffraction method in the determination of crystal structure of crystalline materials: (i) the diffraction profile is characteristic of a given material, (ii) each material in a given composition exhibits its own diffraction profile independently and (iii) the method is

capable of quantitative and qualitative analysis of the phases present in a given mixture. To check and identify the various phases present in (1-x)BF-xSFN ceramics, characterization of calcined and sintered powders was performed using an 18 kW rotating anode (CuKα) based Rigaku (RINT 2000/PC series) powder diffractometer operating in the Bragg-Brentano geometry. X-ray diffraction (XRD) data were collected at slow scan rate of 2 degree/minute at step of 0.02 degree in the two theta range 20 to 120 degrees.

2.3 Introduction to the Rietveld Structure Refinement Method

For the determination of different structural parameters of crystal structure, identification and confirmation of crystal structures and phase analysis of materials, Rietveld method is the most precise tool commonly used in the field of material science when dealing with the polycrystalline sample having powder diffraction patterns. This crystal structure refinement tool was invented by H. M. Rietveld [Rietveld (1967); Rietveld (1969)]. For the refinement of crystal structure of crystalline materials, Rietveld program uses experimental data from neutron, synchrotron or X-ray powder diffraction [Malmros and Thomas (1977); Khattak and Cox (1977); Young (1993)] and try to fit it close to the theoretically calculated diffraction pattern derived from an approximated structural model. So, the knowledge of the basic crystal structure and a starting structural model is important for fitting the diffraction data. If we start with correct structural model and use least square approach in the Rietveld refinement, the theoretical profile is generated in accordance with the initial structural model and tends to overlap the experimentally observed diffraction profiles. Now by tuning the refinable parameters from the instrumental factors and crystal structure, the deviation of theoretically calculated and experimentally observed pattern is minimized to get the best fit up to a satisfactory value. The structural parameters obtained from refined structure giving the satisfactory fit are accepted as the correct crystal

structure. Rietveld analysis minimizes a quantity known as χ^2 [Young (1993)] which is defined by the relation:

$$\chi^2 = \sum w_i \cdot (y_{o,i} - y_{c,i})^2 \qquad \ldots\ldots\ldots\ldots\ldots\ldots (2.1)$$

Where, $y_{o,i}$ and $y_{c,i}$ are experimentally observed and Rietveld calculated diffraction intensities respectively, and $w_i = 1/\sigma_{o,i}^2$ ($\sigma_{o,i}^2$ denotes the variance of the experimentally observed data [Young (1993); Prince (2004); David (2004); Toby (2006)]. Different agreement factors are taken to justify the quality of fits between observed and Rietveld calculated diffraction profiles quantitatively. The weighted profile R-factor, denoted by R_{wp}, which tells about the goodness of fit between observed and calculated diffraction profiles is the square root of the ratio of χ^2 to the weighted intensities [Young (1993); Toby (2006)] written as

$$(R_{wp})^2 = \sum w_i \cdot (y_{o,i} - y_{c,i})^2 / \sum w_i \cdot (y_{o,i})^2 \qquad \ldots\ldots\ldots\ldots (2.2)$$

Other agreement factor associated with Rietveld refinement is expected R-factor (R_{exp}) which is defined as [Young (1993), Toby (2006)]

$$(R_{exp})^2 = N / \sum w_i \cdot (y_{o,i})^2 \qquad \ldots\ldots\ldots\ldots\ldots\ldots\ldots (2.3)$$

Where, N, stands for the number of data points. Now, χ^2 can be written in terms of the two R-factors as

$$\chi^2 = (R_{wp}/R_{exp})^2 \qquad \ldots\ldots\ldots\ldots\ldots\ldots (2.4)$$

For any Rietveld fitting, χ^2 should not decrease below unity. However, if the fitting of data leads to the value of χ^2 less that unity, this means that the value of $<(y_{o,i} - y_{c,i})^2>$ becomes lower than $\sigma^2(y_{o,i})$. This situation may come sometimes when the fitting of the data is performed by overestimating the standard uncertainties or including extra parameters in the refinement. In such cases Rietveld program is forced to fit the noise

which in turn reduces the value of χ^2 less than 1. Generally this kind of situations arises in the fitting of powder diffraction data [Toby (2006)] which can be corrected by taking into account these factors. Further, if χ^2 is very large than 1, this means either the standard uncertainties in the refinement are underestimated or the considered structural model is incorrect [Toby (2006)]. Moreover, if χ^2 comes very close to 1, it does not essentially imply that the considered model or corresponding fit is correct. Different structural models can result into similar fitting due to inadequate or poor diffraction data [Toby (2006)]. To estimate the diffraction profiles via Rietveld method, various kind of functions have been defined in the program. But crystallographers extensively use Pseudo-Voigt function to model the shape of diffraction profiles. Pseudo-Voigt function (pV(x)) is the linear combination of Lorentzian (L(x)) and Gaussian (G(x)) functions written as

$$pV(x) = \eta L(x) + (1-\eta)G(x) \qquad \ldots\ldots\ldots\ldots\ldots .(2.5)$$

The width of diffraction peaks, also known as full width at half maximum (FWHM)), depends on the diffraction angle 2θ and the instrumental parameters. Gaussian component [Mc-Cusker et al. (1999); Carvajal (2001)] of the FWHM is defined by the following equation

$$FWHM = U\tan^2\theta + V\tan\theta + W \qquad \ldots\ldots\ldots\ldots \ldots\ldots\ldots..(2.6)$$

Where, U, V and W are refinable parameters. Lorentzian component is defined [Mc-Cusker et al. (1999); Carvajal (2001)] as

$$FWHM = X\tan\theta + Y/\cos\theta \qquad \ldots\ldots\ldots\ldots\ldots..\ldots\ldots\ldots\ldots (2.7)$$

The parameters U, V and W are different for different diffractometer. But these parameters are nearly fixed for a particular diffractometer, if the effect of line broadening does not contribute to the diffraction data.

2.4 Synthesis of (1-x)BiFeO$_3$-xSr(Fe$_{0.5}$Nb$_{0.5}$)O$_3$

Phase pure (1-x)BF-xSFN compositions were synthesized by solid state reaction method. To determine the structure-property correlations and phase transitions in (1-x)BF-xSFN solid solution, we prepared the samples with the compositions x = 0.10, 0.15, 0.20, 0.25, 0.30, 0.33, 0.36, 0.40, 0.50, 0.60, 0.70, 0.75, 0.80, 0.85, 0.90 and 1.0 (SFN). The sequence of synthesis steps adopted to avoid the formation of impurities in various compositions of (1-x)BF-xSFN solid solution are described in the following sections.

2.4.1 Precursors

Analytical reagent grade reactants Bi$_2$O$_3$ (99.9%, Sigma Aldrich), Fe$_2$O$_3$ (99%, Sigma Aldrich), SrCO$_3$ (99.9%, Alfa Aesar) and Nb$_2$O$_5$ (99.95%, Himedia) were taken as the starting raw materials in the present work. The reactants were characterized for phase purity by XRD before using them. The XRD patterns of the reagents used, Bi$_2$O$_3$, Fe$_2$O$_3$, SrCO$_3$ and Nb$_2$O$_5$, are shown in Fig. 2.1. Comparison of the XRD patterns of various reactants with the ICDD database confirms that they are free from any impurity.

2.4.2 Mixing and Milling

The reactant materials were taken in stoichiometric ratio and mixed properly using an agate mortar-pestle with AR grade acetone as the mixing medium. This mixture was transferred to zirconia jar containing zirconia balls of 5mm as the milling medium.
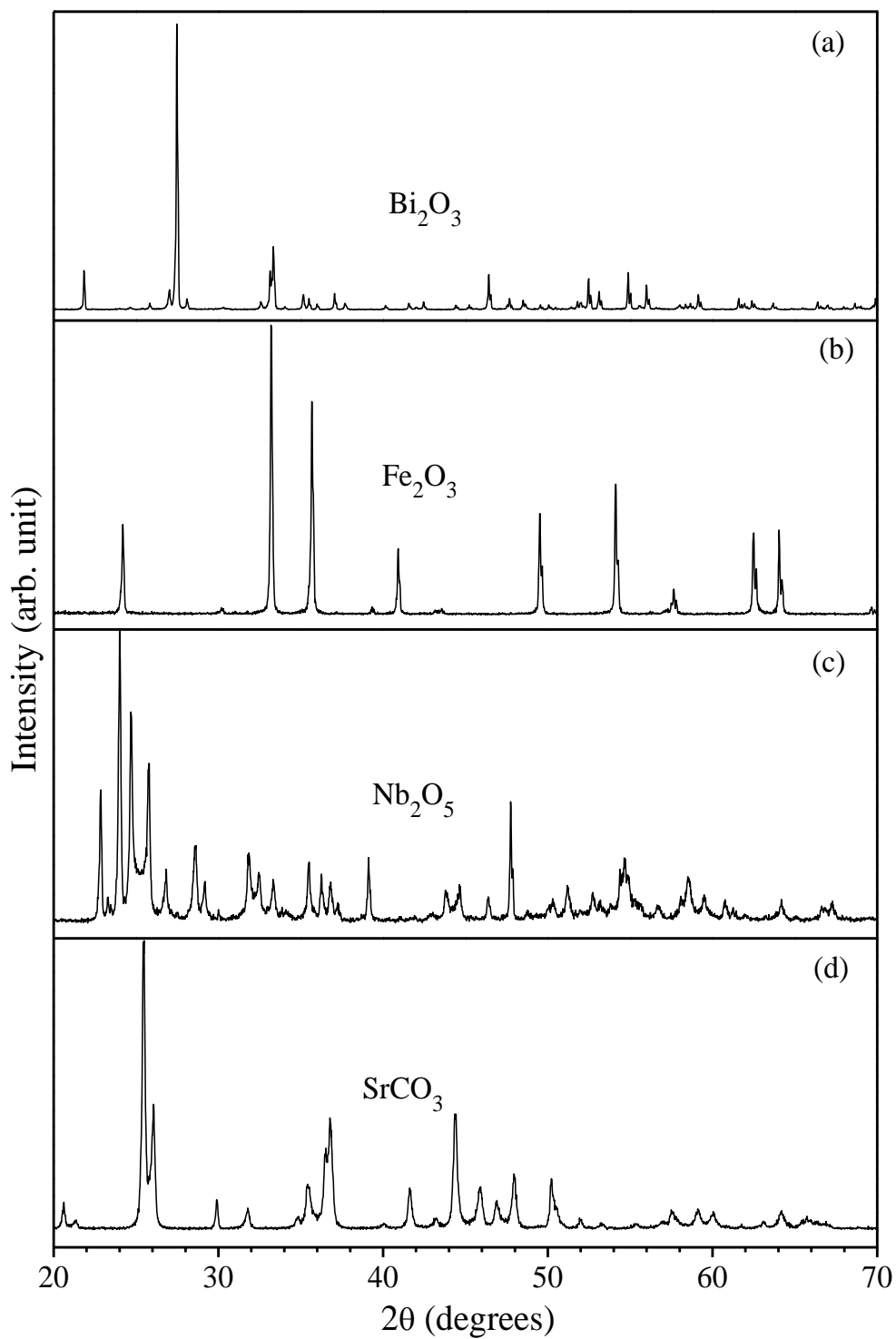
Figure 2.1 X-ray diffraction patterns of the reactants used for synthesis of the $(1-x)BiFeO_3-xSr(Fe_{0.5}Nb_{0.5})O_3$ samples (a) Bi_2O_3 (b) Fe_2O_3 (c) Nb_2O_5 and (d) $SrCO_3$.

Now, AR grade acetone was added in the jar and then ball milling was (Retsch GmbH & Rheinische, Germany) carried out for six hours to get the homogeneous mixture of powders.

2.4.3 Calcinations

After homogeneous mixing of reactant powders in Ball Mill the acetone was evaporated in open air. The dried powder was divided into several parts and used for calcinations to optimize the calcination temperature and time. The calcinations were carried out in an alumina crucible at different temperature by using globar furnace capable of going up to ~ 1600 K. To study the reaction mechanism and optimization of the synthesis process, we have initially selected 0.90BF-0.10SFN composition for calcinations. The ball milled powder was divided into three parts and calcined at 1073 K, 1083 K and 1093 K for 6 hours. The calcined powder was grind to make fine powders using an agate mortar and pestle and then used for the collection of x-ray diffraction patterns. The x-ray diffraction patterns of 0.90BF-0.10SFN powder calcined at different temperatures are presented in Fig. 2.2. A comparison of the x-ray diffraction patterns shown in Fig.2.2 with the XRD patterns of reactants shown in Fig.2.1 suggests that there are no reflections of ingredient powders Bi_2O_3, Fe_2O_3, $SrCO_3$ and Nb_2O_5 in the XRD pattern. It means reactions are completely taken place. Most of the peaks in the XRD pattern of calcined powders shown in Fig.2.2 can be indexed by the perovskite structure for 0.90BF-0.10SFN. There are some additional weak reflections in Fig.2.2 which correspond to the impurity phases of $Bi_2Fe_4O_9$ and $BiNbO_4$. The reflections corresponding to the impurity phase $Bi_2Fe_4O_9$ (ICDD No. 01-072-1832) and $BiNbO_4$ (ICDD No. 00-015-0504) are indicated by asterisks (*) and (#) symbols, respectively. The small peak located at the $2\theta \sim 37.5°$ in Fig.2.2 is due to the cell doubling of the main perovskite phase and is termed as superlattice reflection (S).
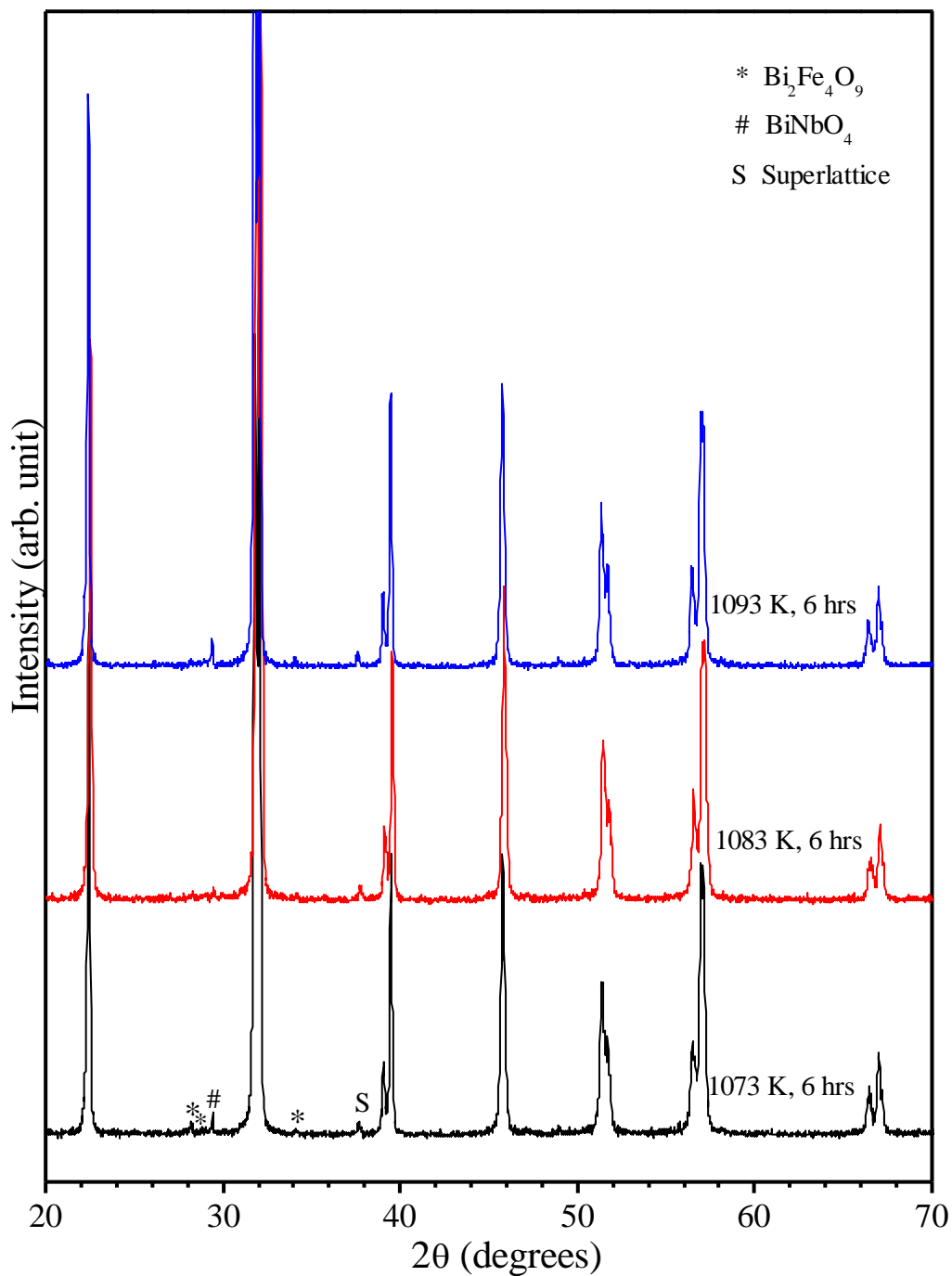
Figure 2.2 The XRD patterns of $0.90BiFeO_3$-$0.10Sr(Fe_{0.5}Nb_{0.5})O_3$ powders calcined at different temperatures for 6 hours. XRD Patterns are zoomed vertically to see the presence of impurity reflections if any.

It is evident from Fig. 2.2 that, as the calcination temperature is increased from 1073 K to 1083 K intensities of the peaks corresponding to the impurity phase get significantly reduced. On further increasing the calcination temperature to 1093 K, the intensity of impurity phase is found to increase again. The superlattice reflection is observed in pure $BiFeO_3$ also and its doped compounds because of anti-phase rotation of oxygen octahedral along the [111] direction of the perovskite structure. Hence 1083 K temperature was taken as the optimum calcination temperature for the 0.90BF-0.10SFN composition. The calcination temperatures for other SFN rich compositions were optimized following the same procedure as for 0.90BF-0.10SFN. The optimized calcinations temperature for 0.80BF-0.20SFN composition was found to be 1113K keeping similar synthesis conditions as that for 0.90BF-0.10SFN. The optimum calcination temperatures for (1-x)BF-xSFN compositions were found to be increasing by an increment of 20 K for every 10% increment of SFN doping. Thus, the optimized calcinations temperatures for (1-x)BF-xSFN compositions investigated in the present work with x = 0.10, 0.20, 0.30, 0.40, 0.50, 0.60, 0.70, 0.80, and 0.90 were found to be 1083, 1113, 1133, 1155, 1175, 1195, 1215, 1235 and 1255 K, respectively. The optimum calcination time for these compositions was 6 hours. The optimum calcination temperature for SFN was found to be 1373 K with somewhat longer calcination time of 12Hrs. The XRD patterns of the calcined powders of (1-x)BF-xSFN for various compositions are shown in Fig. 2.3 and 2.4. These XRD diffraction patterns show that intensity of XRD peak around 29.5^o corresponding to the very small impurity phase continuously decreases as the doping concentration of SFN increases in the solid solution. Formation of the impurity phase is eliminated for the compositions with SFN higher than x = 0.40.
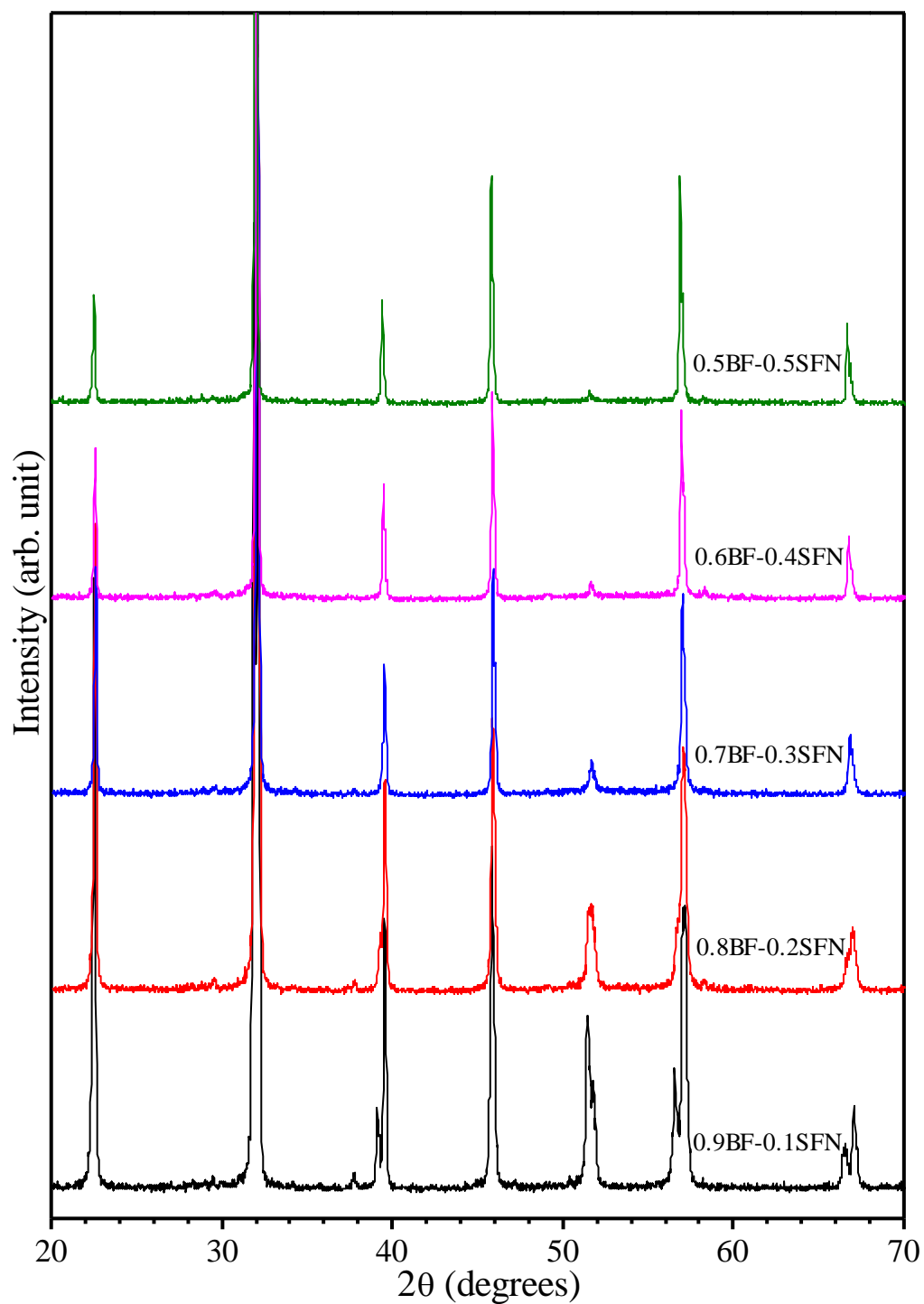
Figure 2.3 XRD patterns of the calcined $(1-x)BiFeO_3-xSr(Fe_{0.5}Nb_{0.5})O_3$ powders with x = 0.10, 0.20, 0.30, 0.40 and 0.50. The weak impurity peak at 29.5^o is seen to be eliminated for higher SFN concentrations.
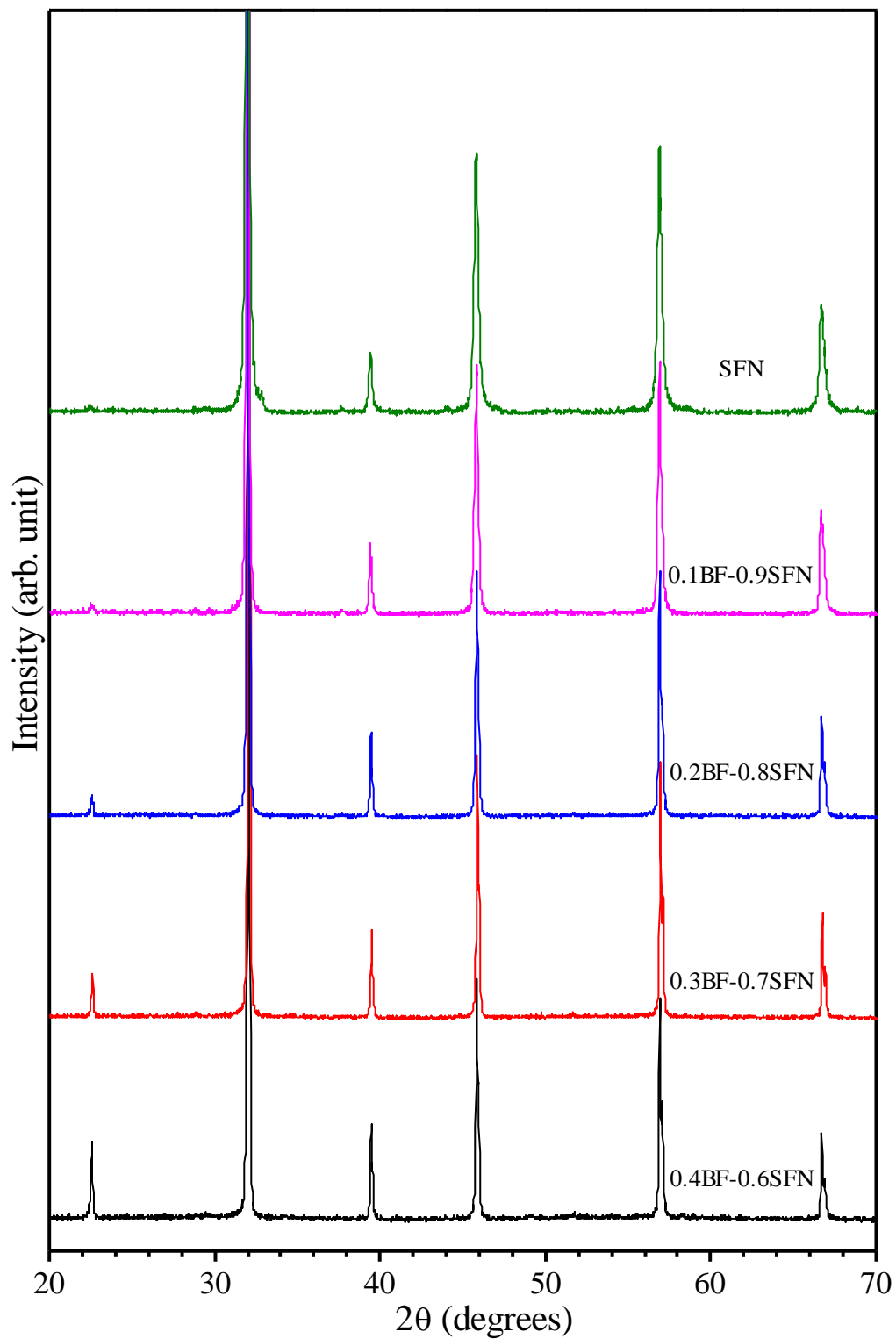
Figure 2.4 XRD patterns of the calcined $(1-x)BiFeO_3-xSr(Fe_{0.5}Nb_{0.5})O_3$ powders with $x = 0.60, 0.70, 0.80, 0.90,$ and 1.00 compositions.

2.4.4 Preparation of Green Pellets

After calcination, the prepared sample was properly crushed and well mixed with an organic binder of 2% polyvinyl alcohol (PVA) solution in distilled water using agate mortar pestle. PVA solution mixed powder was used for the preparation of green pellets. Green pellets of (1-x)BF-xSFN ceramic were made with the help of a cylindrical stainless steel die of 1.2 cm diameter. Before making pellets, die was properly cleaned and its inner surface was slightly wet with the help of stearic acid solution to act as lubricant. This reduced the friction and avoids sticking of the powder on the inner surfaces of the die. Now we put the calcined powder and press to convert it into the form of pellet. The calcined powder was kept in the die uniaxially pressed at an optimized load of 65 kN using hydraulic press.

2.4.5 Sintering

Before sintering, the green pellets were annealed at 774 K for ten hrs to completely burn-off the organic binder (PVA). Since Bi-is volatile at higher temperatures, evaporation of Bi-oxide during sintering may affect the stoichiometry of the samples. In view of this, sintering of pellets was performed inside sealed alumina crucible having small amount of sacrificial calcined powder of same composition range $0.1 \leq x \leq 0.90$. The vapour pressure of Bi-oxide evaporated from the loose calcined powder counterbalances escape of Bi-oxide from the pellets and prevents the loss of bismuth during sintering. The sintering temperatures of the end components of the (1-x)BF-xSFN solid solution are known to be quite different. The pure SFN is sintered at relatively higher temperatures while the pure BF is sintered at lower temperatures as Bi-oxide acts as sintering aid also. We optimized the sintering temperature and time of pure SFN to be ~ 1623 K for 5 hours and 30 minutes, respectively for getting maximum densification. The optimum sintering

temperature for pure BF is ~ 1173 K for 1 hour duration. Therefore, the sintering temperature and time for (1-x)BF-xSFN solid solutions were increased with increasing the doping concentration of SFN. The optimized sintering temperatures for x = 0.10, 0.20, 0.30, 0.4, 0.5, 0.6, 0.7, 0.8 and 0.90 are 1193, 1213, 1238, 1268, 1298, 1333, 1373, 1418 and 1523 K respectively. The sintering time was varied accordingly, for lower composition starting from 1 hour to higher composition for 5 hour. The green pellets of various compositions were sintered at optimum temperature and time and then crushed into fine powders for XRD characterization. The crushed powders were annealed at 773 K for 10 hours to remove strains which may develop during the process of crushing. This annealed powder was used for collecting the x-ray powder diffraction data. The XRD patterns of sintered (1-x)BF-xSFN powders with compositions x = 0.10, 0.15, 0.20, 0.25, 0.30, 0.33, 0.36, and 0.4 are given in Fig. 2.5, while for x = 0.50, 0.60, 0.70, 0.75, 0.80, 0.85, 0.90 and 1.0 (SFN) are given in Fig. 2.6. The letter 'S' in both the figures represents the superlattice reflections appearing due to cell doubling. As can be seen from these figures, all the compositions are free from any impurity phase except the compositions with x=0.10 and 0.15. In fact, the impurity peaks are barely visible due to their negligible phase fraction in the samples.

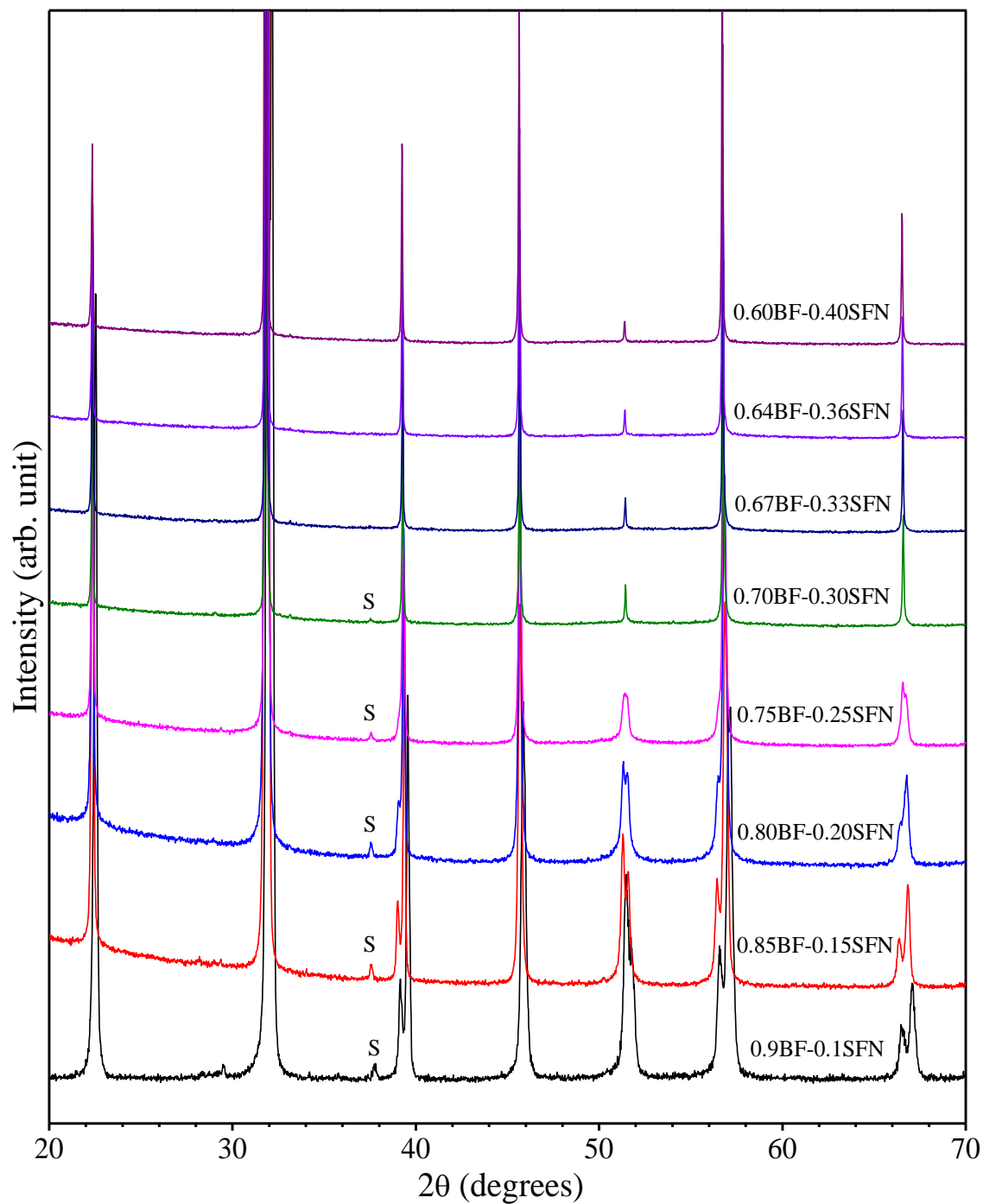**Figure 2.5** XRD patterns of sintered $(1-x)BiFeO_3-xSr(Fe_{0.5}Nb_{0.5})O_3$ samples for compositions x = 0.10, 0.15, 0.20, 0.25, 0.30, 0.33, 0.36 and 0.40. The letter 'S' represents the superlattice reflection.

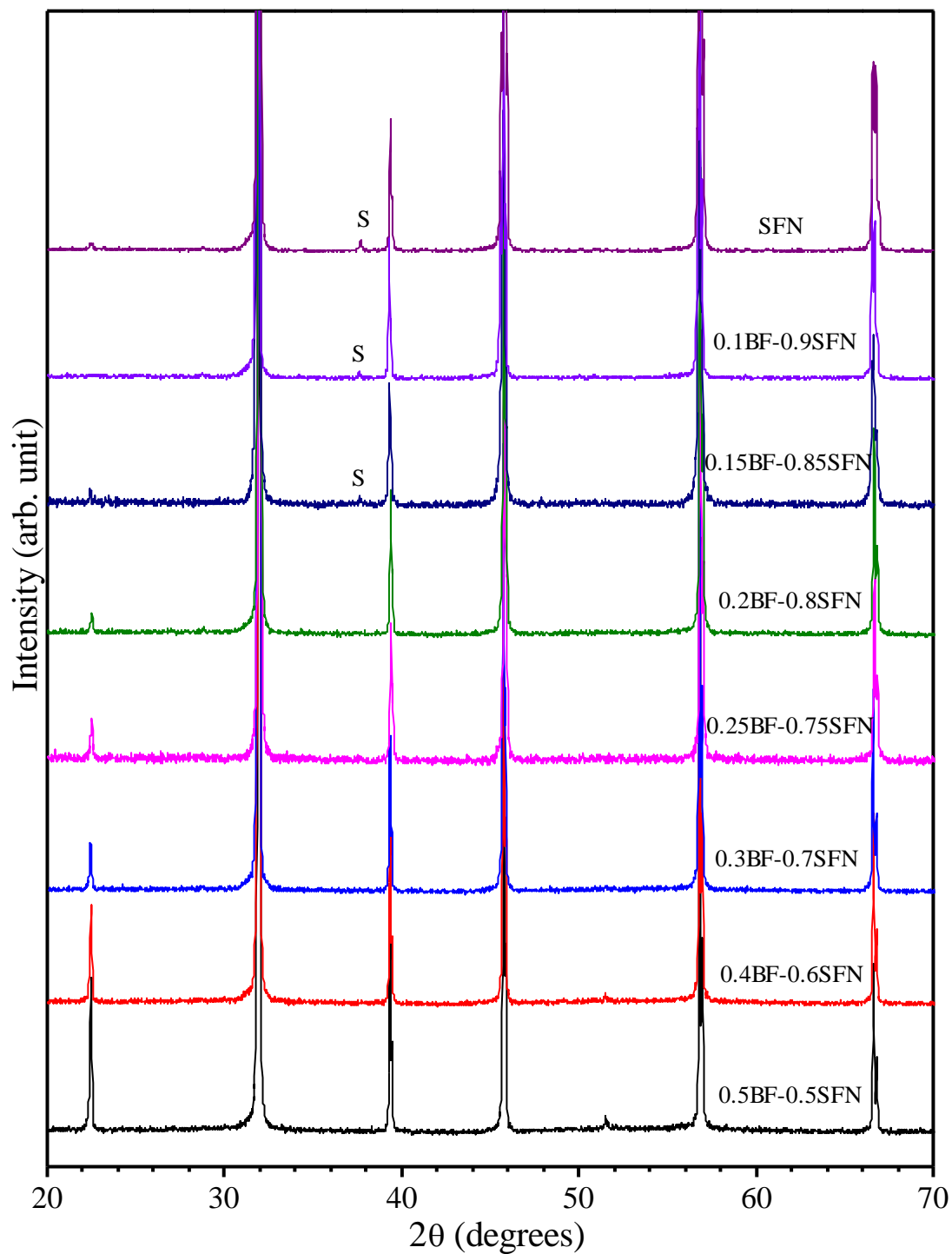**Figure 2.6** XRD patterns of sintered $(1-x)BiFeO_3-xSr(Fe_{0.5}Nb_{0.5})O_3$ samples for the compositions x = 0.50, 0.60, 0.70, 0.75, 0.80, 0.85, 0.90 and 1.00. The letter 'S' represents the superlattice reflection.

2.5 Microstructural and Compositional Study

Scanning electron microscopic analysis was done on the sintered pellet surfaces to study the microstructure and compositional analysis of the (1-x)BF-xSFN samples. Scanning electron microscopy was carried out using high resolution scanning electron microscope (HR-SEM) (Nova NanoSEM 450, FEI) equipped with energy dispersive X-ray spectroscopy (EDS) technique. Fig. 2.7, Fig. 2.8 and Fig. 2.9 depicts the scanning electron micrographs and EDS spectra of (1-x)BF-xSFN ceramics for x = 0.10, 0.30, 0.40; 0.50, 0.80, 0.90; and 1.00, respectively, corresponding to $BiFeO_3$-rich end, middle compositions, SFN-rich end and finally SFN. From these micrographs, it is obvious that the grain size and density of pellets enhances with increase in the doping concentration of SFN. The x = 0.1 composition has some porosity as seen in the micrograph in Fig.2.7. Linear intercept method was used to determine the average grain size. The average grain sizes for x = 0.10, 0.30, 0.40, 0.50, 0.80, 0.90 and 1.00 are approximately 1.12, 4.26, 3.22, 1.5, 1.93, 1.66 and 5.54μm, respectively. The higher grain size for SFN modified compositions is attributed to the higher sintering temperatures. The microstructure of the compositions with x=0.10 and 0.30 are seen to be little bit different from the other compositions. As the compositions with x=0.10 and 0.30 are on the Bi-rich end, due to liquid phase sintering assisted by lower melting temperature Bi-oxide, the surface of these compositions are seen to be having frozen glassy liquid phase on top of the polycrystalline microstructure. Further, the grain growth mechanism for pure SFN (x = 1.00) sample is also quite different (see Fig.2.9). It looks like the individual grain of SFN sample is the result of the stacking of number of thin slice of disk one over other forming nice steps. This type of grain growth occurs due to presence of screw dislocation which forms a growth step at the growing surface of the grain.
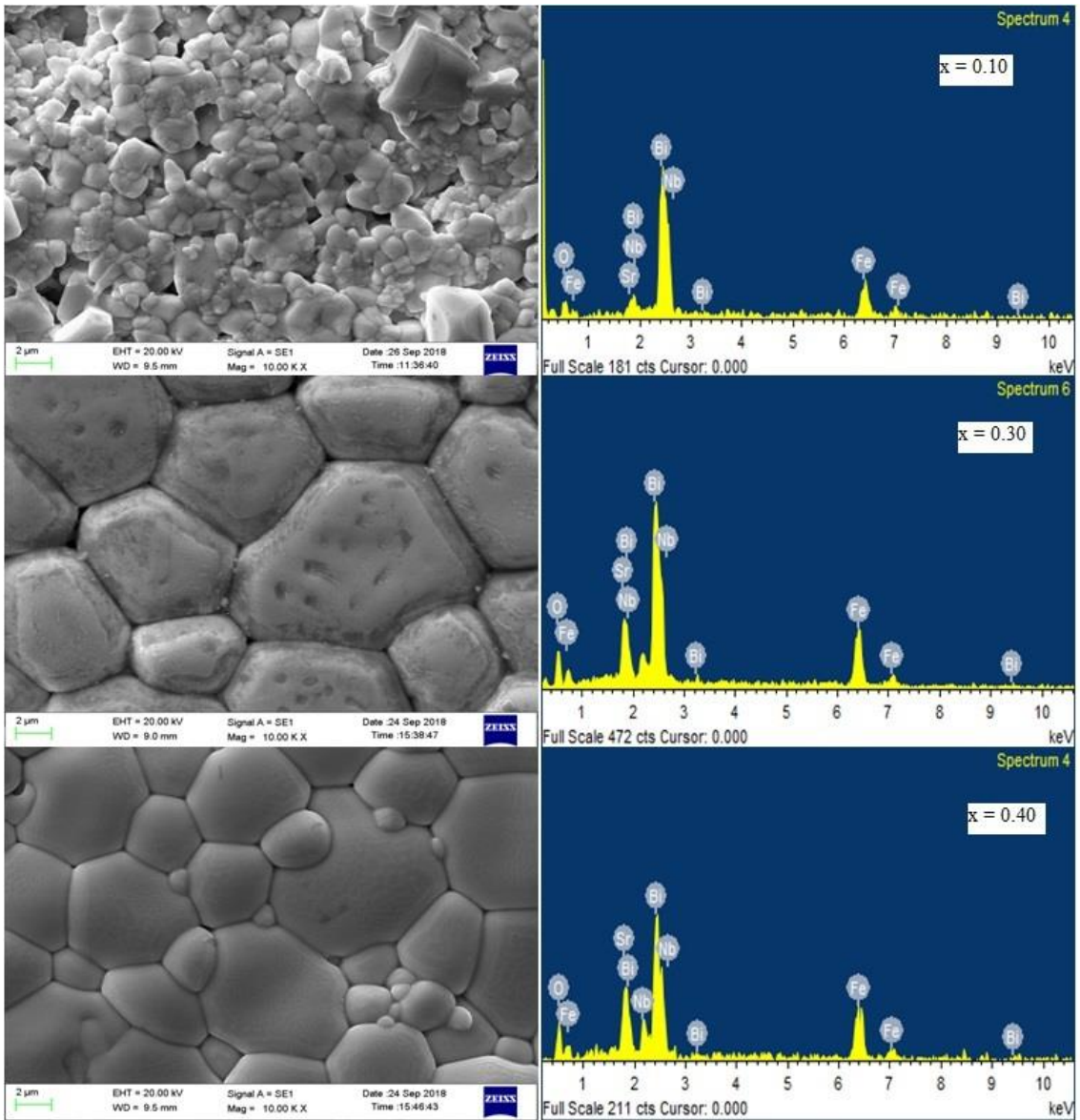
Figure 2.7 Scanning electron micrographs and EDS spectra of $(1-x)BiFeO_3$-$xSr(Fe_{0.5}Nb_{0.5})O_3$ ceramics for x = 0.10, 0.30 and x = 0.40.

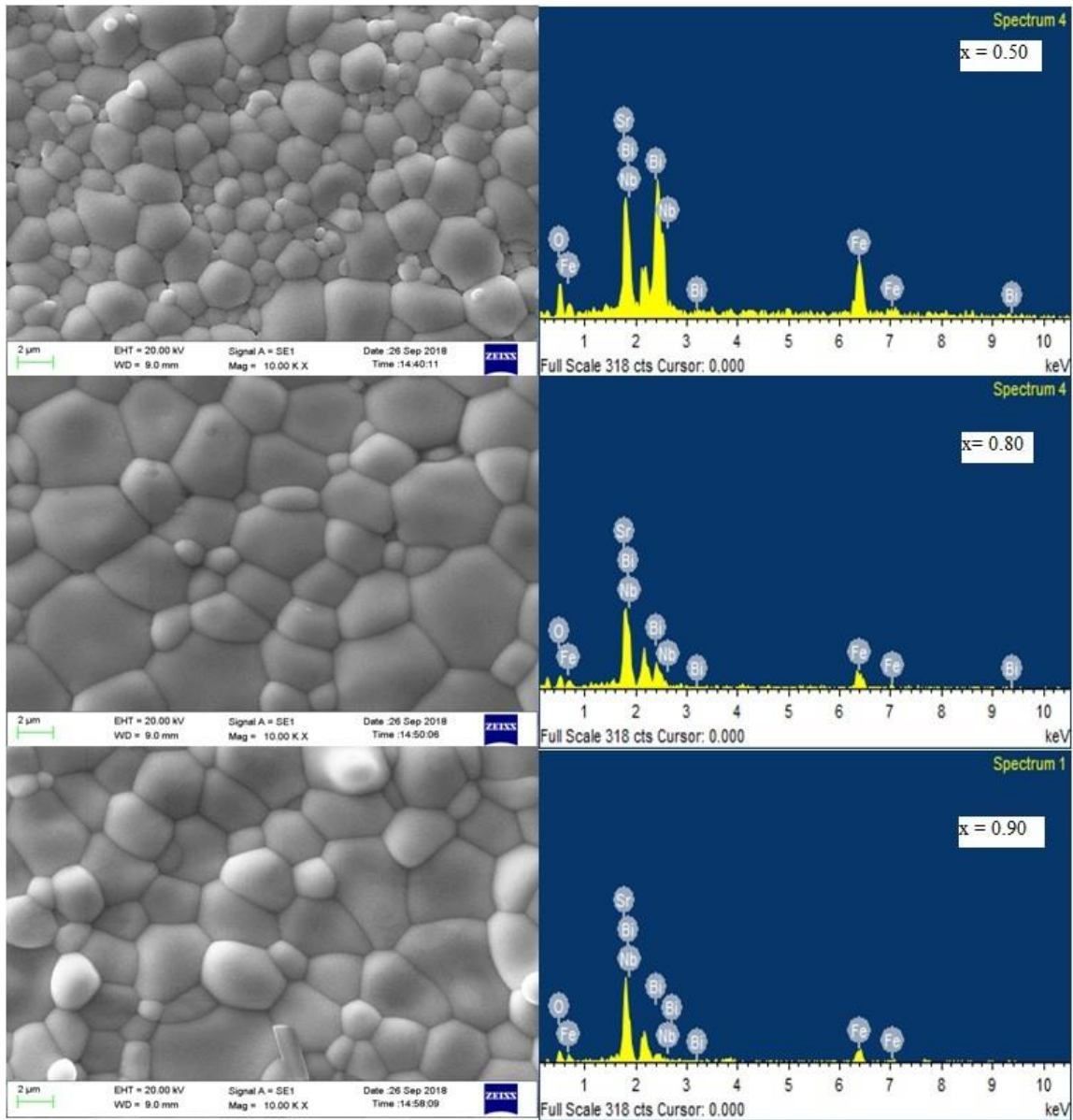**Figure 2.8** Scanning electron micrographs and EDS spectra of $(1-x)BiFeO_3$-$xSr(Fe_{0.5}Nb_{0.5})O_3$ ceramics for $x = 0.50$, 0.80 and 0.90.

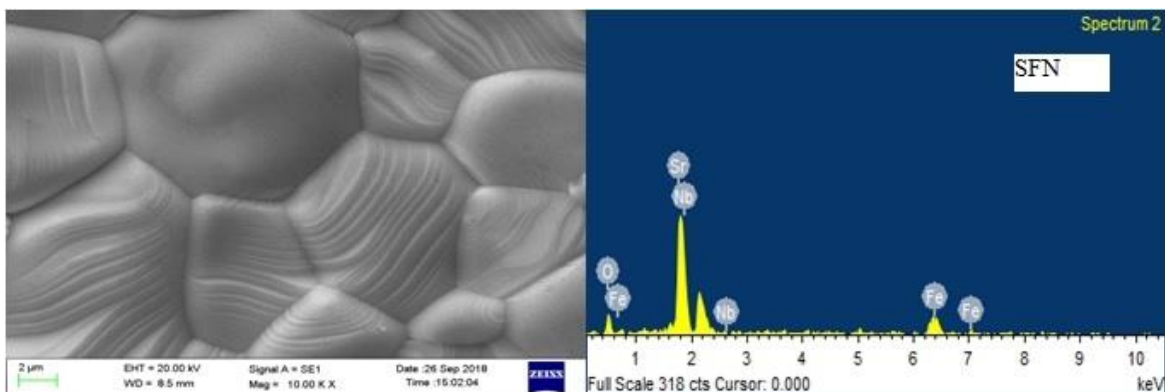**Figure 2.9** Scanning electron micrographs (SEM) and EDX spectra of $Sr(Fe_{0.5}Nb_{0.5})O_3$ ceramics.

The EDS spectra of various compositions of (1-x)BF-xSFN samples are shown in the right panel of the Figs. 2.7, 2.8 and 2.9. It shows that each sample is composed of bismuth (Bi), strontium (Sr), iron (Fe), niobium (Nb) and oxygen (O) atoms. The EDS spectra confirm that no other impurity elements are there in the samples. The calculated atomic percentage of various elements from the EDS analysis along with the atomic percentages as expected from the nominal compositions of the samples are listed in table 2.1 and 2.2. The calculated atomic percentage of various elements from the EDS analysis is close to the atomic percentages expected from the nominal compositions within the experimental error. Since the EDS technique is not very accurate for lower atomic number elements, the average atomic percentages of oxygen atom cannot be determined precisely. This inaccuracy in atomic percent of oxygen atoms also disturbs the atomic percentages of other atoms (Sr, Bi, Fe and Nb) during estimation. The fraction of lower atomic number element like Fe is seen to be underestimated while the higher atomic number element Bi is

77

seen to be overestimated in the EDS analysis. However, the differences in the observed and

nominal atomic percentage values are within the accepted limit of the EDS measurements.

Table 2.1 Results of EDS analysis of $(1-x)BiFeO_3$-$xSr(Fe_{0.5}Nb_{0.5})O_3$ ceramics for $x = 0.10$, 0.30, 0.40, 0.50, 0.80 and 0.90.

	x = 0.10		x = 0.30		x = 0.40	
Elements	Nominal atomic%	Experimental atomic%	Nominal atomic%	Experimental atomic%	Nominal atomic%	Experimental atomic%
O K	60	57.65	60	60.40	60	59.71
Fe K	19	18.76	17	15.97	16	15.55
Sr L	2.00	1.65	6	5.63	8	7.17
Nb L	1.00	1.08	3	3.50	4	4.89
Bi M	18	20.87	14	14.50	12	12.67

	x = 0.50		x = 0.80		x = 0.90	
Elements	Nominal atomic%	Experimental atomic%	Nominal atomic%	Experimental atomic%	Nominal atomic%	Experimental atomic%
O K	60	58.97	60	59.30	60	61.25
Fe K	15	14.21	12	10.50	11	9.84
Sr L	10	10.48	16	15.99	18	16.41
Nb L	5	6.02	8	9.29	9	10.39
Bi M	10	10.32	4	4.91	2	2.12

Table 2.2 Results of EDS analysis for $Sr(Fe_{0.5}Nb_{0.5})O_3$ ceramics.

SFN		
Elements	Nominal atomic%	Experimental atomic %
O K	60	64.38
Fe K	10	7.31
Sr L	20	17.76
Nb L	10	10.55

2.6 Conclusions

Various compositions of phase pure $(1-x)BiFeO_3-xSr(Fe_{0.5}Nb_{0.5})O_3$ solid solution were successfully synthesized under optimized synthesis conditions using conventional solid state ceramic method. The synthesized samples were free from the impurity phases such as $Bi_2Fe_4O_9$, $Bi_{25}FeO_{39}$ and $Bi_{36}Fe_2O_{57}$ which are reported to commonly form during different stages of synthesis in $BiFeO_3$ based solid solutions. The solid solution formation of $BiFeO_3$ with $Sr(Fe_{0.5}Nb_{0.5})O_3$ has been found to be very effective in suppressing the formation of impurity phases. The average grains size of the samples prepared under optimized conditions were found to be in the range of ~1.1 to ~5.5μm. The EDS analysis confirms compositional homogeneity of the samples.